Benzothiadiazolyl-pyridine and -2,2'-bipyridine Ligands for Luminescent and Magnetic Complexes

Nataliya Plyuta, Thomas Cauchy, Miguel Julve, Narcis Avarvari

Benzothiadiazolyl-pyridine and -2,2'-bipyridine ligands for luminescent and magnetic complexes†‡

Dr. Nataliya Plyuta,[a] Dr. Thomas Cauchy,[a] Prof. Miguel Julve[b] and Dr. Narcis Avarvari*[a]

[a] *Univ Angers, CNRS, MOLTECH-Anjou, SFR MATRIX, F-49000 Angers, France. E-mail: narcis.avarvari@univ-angers.fr*

[b] *Instituto de Ciencia Molecular (ICMol)/Departament de Química Inorgànica, Universitat de València, C/ Catedrático José Beltrán 2, 46980 Paterna (València), Spain*

†Electronic supplementary information (ESI) available: Figures S1-S53, Tables S1-S34). CCDC reference number 2277636–2277642 contain the supplementary crystallographic data for this paper. These data can be obtained free of charge via www.ccdc.cam.ac.uk/data_request/cif, or by emailing data_request@ccdc.cam.ac.uk, or by contacting The Cambridge Crystallographic Data Centre, 12 Union Road, Cambridge CB2 1EZ, UK; fax: +44 1223 336033.

‡Dedicated to Professor Marc Sallé on the occasion of his 60th anniversary

Abstract

Two new luminescent ligands, 4-(2-pyridine)-7-methyl-2,1,3-benzothiadiazole (L^1) and 4-(2,2-bipyridine)-7-methyl-2,1,3-benzothiadiazole (L^2), based on 2,1,3-benzothiadiazole and pyridine or bipyridine were obtained by Suzuki coupling reactions. DFT and TD-DFT type calculations have been performed on L^1 and L^2 in order to assign their experimental UV-visible and emission bands. Reaction of L^1 and L^2 with metal(II) chlorides (M = Zn, Mn, Cu) provided the neutral complexes of formulas $[ZnL^1Cl_2]$ (**1**), $[Zn(L^1)_2Cl_2]$ (**2**), $[ZnL^2Cl_2]$ (**3**), $[MnL^2Cl_2]\cdot 0{,}5CH_2Cl_2$ (**4**) and $[CuL^2Cl_2]\cdot H_2O$ (**5**) which have been structurally characterized. The Zn(II) ions in **1** and **2** are four-coordinate in somewhat distorted tetrahedral N_2Cl_2 surroundings with L^1 adopting bidentate (**1**) and monodentate (**2**) coordination modes. Complexes **3**-**5** are isostructural and their metal atoms are five-coordinate in distorted square pyramidal environments with three nitrogen atoms from the tridentate L^2 ligand and a chlorine building the basal plane and another chlorine atom occupying the apical position. The three Zn(II) complexes are strongly luminescent in solution and the solid state, while the cryomagnetic study of the paramagnetic compounds **4** and **5** in the temperature

range 2.9-300 K shows a Curie-Weiss behaviour typical of small antiferromagnetic interactions which are mediated by weak intermolecular contacts.

Introduction

The association of 2,1,3-benzothiadiazole (BTD), a well-known electron acceptor fluorophore,[1,2] with coordinating motifs allows the preparation of functional ligands providing luminescent metal complexes.[3] Although the interest aroused by the BTD unit is especially related to the access to active components for organic electronics,[4-10] redox switchable donor-acceptor systems,[11,12] or its use as synthon in crystal engineering through chalcogen N···S bonding,[13-15] the number of BTD ligands and corresponding metal complexes containing coordinated BTD has been continuously increasing. Accordingly, BTD itself can act as a monodentate monotopic or monodentate ditopic ligand in, for example, Ru(II),[16,17] Cu(II),[18] Cu(I),[18,19] Ag(I), [19,20] Au(I)[21] and Ir(III) [22] complexes. However, when additional coordinating groups are appended in the 4 and 7 positions of the BTD motif, chelating ligands involving the sp^2-hybridized nitrogen atoms of the thiadiazole ring are generated. As such, Pd(II) cyclopalladated complexes of 4-aryl-BTD,[23] a Zn(II) MOF derived from BTD-4,7-dicarboxylic acid,[24] or NIR-emissive tetranuclear Er(III) complexes with 4-hydroxo-2,1,3-benzothiadiazolate,[25] all containing bidentate ligands with the participation of at least one of the nitrogen atoms of the thiadiazole ring, have been described. More recently, we have reported monotopic tridentate Schiff-base BTD ligands resulting from the condensation of 4-amino-BTD with salicylaldehyde and *ortho*-vanillin, together with their Zn(II),[26] Cu(II)[26] and Co(II) complexes,[27] the latter showing field-induced single-ion magnet (SIM) behaviour. A particularly appealing combination is that of BTD with 2-pyridyl units in the 4,7-positions of BTD, providing the bidentate ditopic ligand 4,7-di(2'-pyridyl)-2,1,3-benzothiadiazole [(2'-Py)$_2$BTD in Scheme 1] which is able in principle to afford mononuclear and binuclear metal complexes.

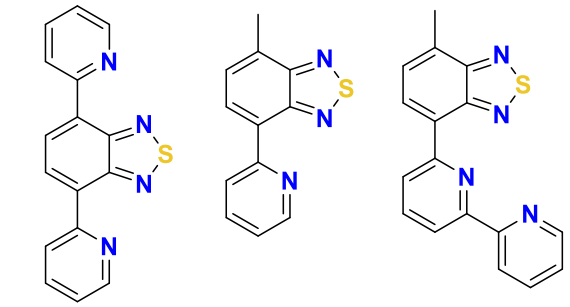

Scheme 1. BTD-pyridine and bipyridine ligands. L^1 and L^2 are described in this work.

(2'-Py)$_2$BTD has been described back in 2004,[28] yet, rather surprisingly, it has not been used as a ligand against metal ions until very recently. Indeed, some of us have reported in 2021 mono- and dinuclear Zn(II) complexes and also dinuclear Ag(I) species, the former ones being luminescent.[29] However, the formation of mononuclear complexes with such ditopic ligands requires a very precise control of the reaction conditions. We describe herein the synthesis and characterization of the Me-BTD monotopic bidentate and tridentate ligands L^1 and L^2 ligands (Scheme 1), containing 2-pyridyl and 2,2'-bipyridyl units respectively, together with their mononuclear Zn(II), Mn(II) and Cu(II) complexes. The photophysical properties of the ligands and of the Zn(II) complexes are described and rationalized by means of DFT and TD-DFT type calculations. Moreover the cryomagnetic properties of the Mn(II) and Cu(II) complexes have been investigated.

Results and discussions

Synthesis and structural characterization of L^1 and L^2

The sp^2-hybridized nitrogen chelating L^1 and L^2 ligands have been synthesized by Suzuki coupling using the Me-BTD derivative of dioxaborolane (**I**) and suitable bromine derivatives of pyridine and 2,2'-bipyridine in the presence of a palladium catalyst and a base (Scheme 2, Figures S1-S4, ESI†).

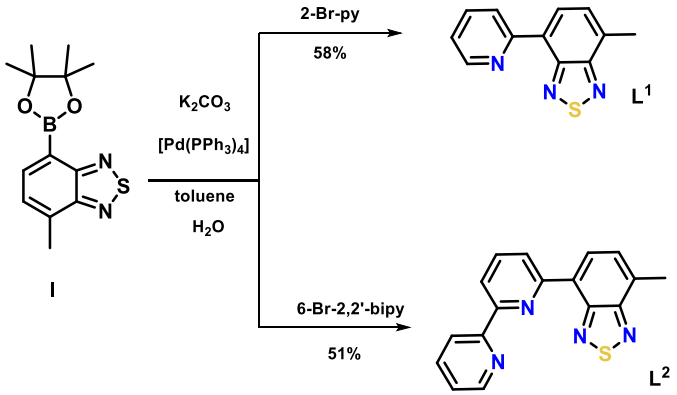

Scheme 2. Synthesis of the new ligands L^1 and L^2.

The precursor **I** was obtained in four steps starting from 2-amino-5-nitrotoluene (**II**) (Scheme 3) and it was then used for the preparation of L^1 and L^2. The first three steps consist of the reduction of the nitro group of **II** to afford the diamino derivative **III**, then its reaction with thionyl chloride leading to the thiadiazole ring in **IV**, followed by the electrophilic bromination of the latter to obtain 4-methyl-7-bromo-BTD (**V**).[30] The last step is a palladium catalyzed reaction of **V** with bis(pinacolato)diboron to afford the dioxaborolane derivative **I**. [31]

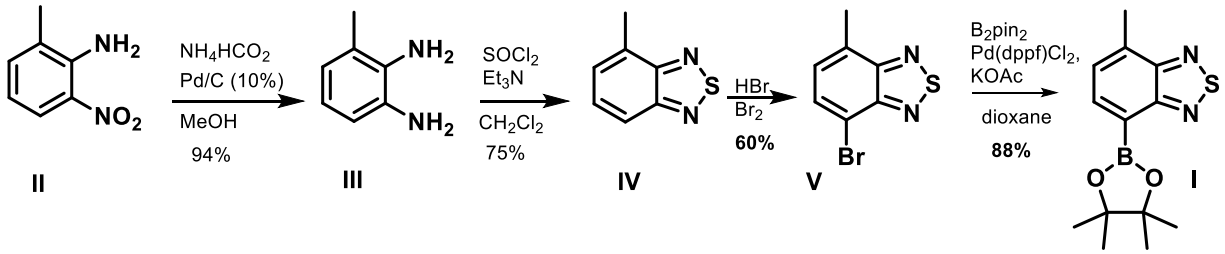

Scheme 3. Synthesis of the precursor **I**.

Both BTD compounds L^1 and L^2 show reversible reduction processes at $E_{1/2}$ = -1.65 V *vs* SCE and $E_{1/2}$ = -1.68 V *vs* SCE, respectively (Figure S12, ESI†), corresponding to the formation of the thiadiazolyl anion.

Suitable single crystals of ligands L^1 and L^2 for X-ray diffraction analysis have been obtained by slow evaporation of dichloromethane solutions. L^1 and L^2 crystallized in the monoclinic $P2_1/n$ space group, with one independent molecule in the asymmetric unit (Tables S2-S4, ESI†). The BTD part adopts an *anti*-conformation with respect to the pyridyl or bipyridyl rings, with values for the N3C8C6C1 torsion angles of 174.3 and 172.9° for L^1 and L^2, respectively (Figure 1). The adjacent molecules of these ligands are connected by π-π interactions [values of the

centroid···centroid distances of 3.84 or 3.5 Å (L^1) and 3.83 or 3.5 Å (L^2)], forming rows with stacking structures. Each two rows are linked by weak S···S contacts of 3.649 (L^1) and 3.322 Å (L^2) (Figure S13, ESI†).

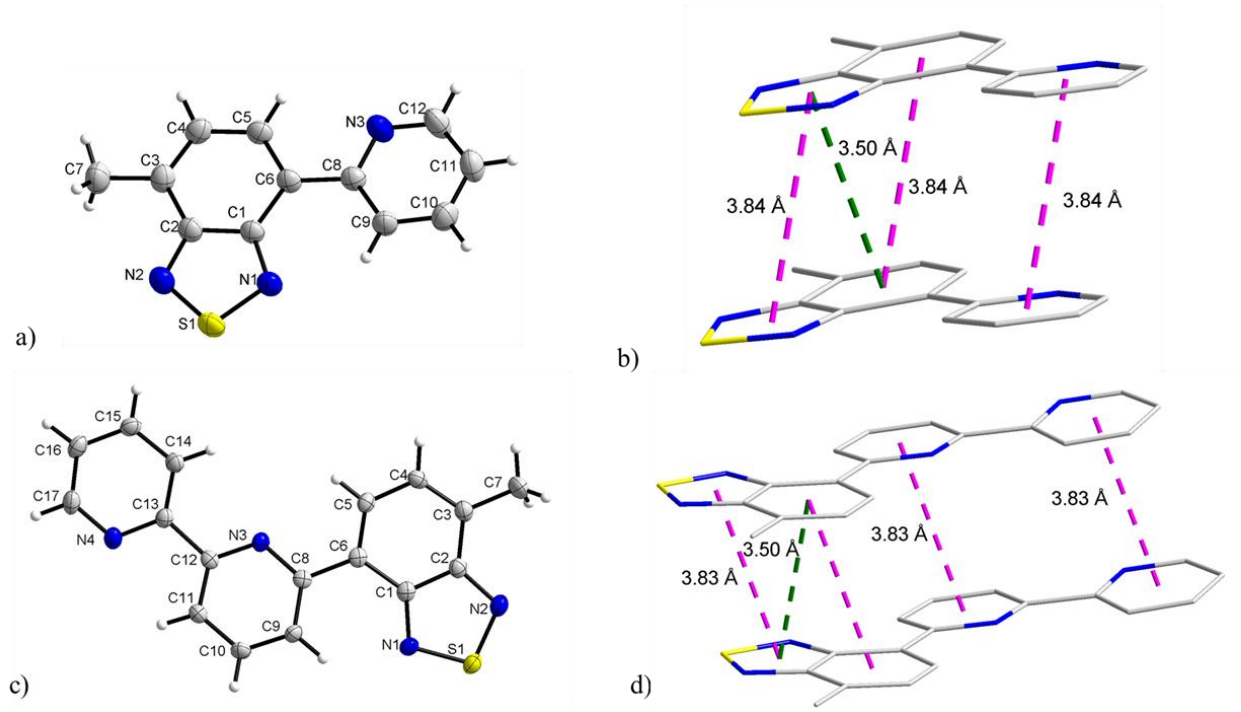

Figure 1. Molecular structures (with the numbering scheme and displacement ellipsoids drawn at the 50% probability level) and views of fragments of the crystal packing with highlighted π-π interactions (dotted lines) for L^1 (a and b) and L^2 (c and d).

DFT calculations on L^1 and L^2

Density Functional Theory (DFT) calculations were performed for geometry optimizations and electronic parameters (see computational details). Starting geometries for the ligands L^1 and L^2 were derived from the X-ray structures. Upon optimization, the calculated bond lengths and angles were in good agreement with the experimental geometries. The main difference concerns the planarity of the ligands. The calculated value of the N3C8C6C1 angle is close to 180 ° (exp. 174.33 °) for L^1 and amounts at 163.1 ° (exp. 172.96 °) in the case of L^2. We have also performed DFT calculations on the ligands with *cis*- and *trans*-conformations. The most stable form is the *trans* one for both ligands, like in the X-ray structures. The total molecular energy differences are 3.78

and 9.40 kcal mol^{-1} for L^1 and L^2, respectively (see Table 1). In the following, the experimental data will be compared with the calculated data of these forms.

Table 1. Calculated dihedral angles and total molecular energies for the different conformations of L^1 and L^2

Angle, deg	L^1		L^2			
	trans	*cis*	*trans-trans*	*cis-trans*	*trans-cis*	*cis-cis*
C1C6C8N3	179.9	45.1	163.1	-42.1	172.5	46.8
N3C12C13N4	-	-	175.9	-175.3	33.7	38.4
ΔE, kcal/mol	0	3.78	0	2.75	5.02	9.40

The HOMO and LUMO pictures for L^1 and L^2 are shown in Figure 2. The values of the LUMO energies for both ligands are quite low and the largest contributions are localized on the BTD moiety, in agreement with its electron-withdrawing properties. The topologies and energies of the frontier molecular orbital for L^1 and L^2 are quite the same. Replacing a pyridyl ring in L^1 with a 2,2'-bipyridyl in L^2 seems to have a small effect on the electronic properties of the ligand, with a very weak donating effect on the energy values of the HOMO. The HOMO delocalizes on the whole molecule in L^1 and mostly on BTD and the adjacent pyridyl ring in L^2.

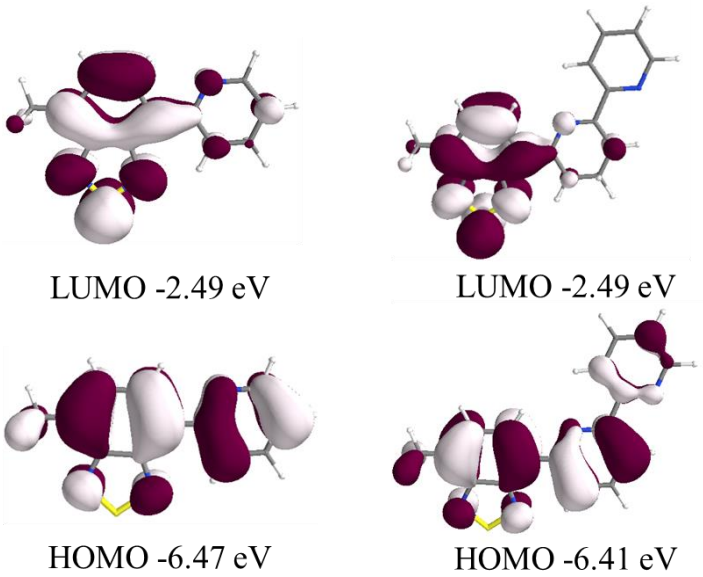

Figure 2. HOMO's and LUMO's of **L^1** (left) and **L^2** (right).

Coordination of L^1 and L^2 with M(II) centres (M = Zn, Mn, Cu)

The metal precursors zinc(II) chloride, manganese(II) chloride tetrahydrate and copper(II) chloride dihydrate were used herein to investigate the coordination ability of L^1 and L^2. The complex of formula $[ZnL^1Cl_2]$ (**1**) was obtained through the reaction between L^1 and an excess of $ZnCl_2$ in a mixture of methanol and dichloromethane at room temperature. By slightly changing the reaction conditions, upon heating at 65 °C L^1 with $ZnCl_2$ in a 1:1 molar ratio, $[Zn(L^1)_2Cl_2]$ (**2**) has been exclusively obtained. Moreover, in the case of L^2, the complexes of formulas $[ZnL^2Cl_2]$ (**3**), $[MnL^2Cl_2]\cdot 0.5CH_2Cl_2$ (**4**) and $[CuL^2Cl_2]\cdot H_2O$ (**5**) have been prepared in the same conditions (Scheme 4).

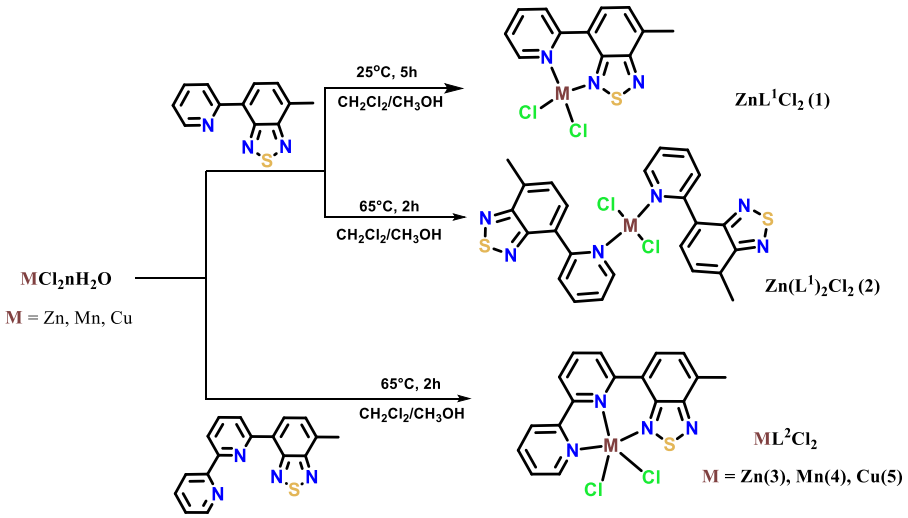

Scheme 4. Synthetic route for complexes **1** - **5**.

The NMR spectra of L^1, L^2 and their zinc(II) complexes have been recorded in $CDCl_3$ or CD_2Cl_2 (Figures S1-11, Table S1). In all spectra of complexes we observed shifts in the signals compared to the free ligands, what confirms coordination of the ligand in the solution.

X-ray quality crystals have been obtained for all complexes, i.e. $[ZnL^1Cl_2]$ (**1**), $[Zn(L^1)_2Cl_2]$ (**2**), $[ZnL^2Cl_2]$ (**3**), $[MnL^2Cl_2]\cdot 0.5CH_2Cl_2$ (**4**) and $[CuL^2Cl_2]\cdot H_2O$ (**5**), by slow evaporation of dichloromethane/methanol solutions (Table S5, ESI†).

Complexes **1**, **3**, **4** and **5** crystallize in the centrosymmetric monoclinic *C*2/*c* space group and the asymmetric unit is composed of one independent molecule of the complex (**1**, **3**, **4** and **5**) and solvent molecules of crystallization, dichloromethane (**4**) or water (**5**). Compound **2** crystallizes in the centrosymmetric orthorhombic *Pbcn* space group, with half a molecule of complex in the asymmetric unit, the other half being generated by the two-fold axis crossing the metal ion.

L^1 adopts *cis*- and *trans*-conformations, adopting monodentate and bidentate coordination modes in **1** and **2**, respectively. The zinc ions in these two compounds are four-coordinate with N_2Cl_2 environments which are built by two chloride ions (**1** and **2**) and one thiadiazolyl and one pyridyl nitrogen atoms from one L^1 molecule (**1**), and two pyridyl nitrogen atoms from two molecules of L^1 (**2**). The coordination geometry of each zinc(II) is distorted tetrahedral with $\tau_4 = 0.93$ and 0.90[32] for **1** and **2**, respectively (Fig. 3 and 4 and Tables 2, S6 and S7, ESI†).

Table 2. Selected geometrical parameters (Å, deg) and the BVS values for the complexes **1-5**

	1	**2**	**3**	**4**	**5**
M-Cl	2.2115(11)	2.2413(13)	2.2773(5)	2.3654(10)	2.2968(10)
	2.2076(12)		2.3261(5)	2.3966(10)	2.4699(11)
M-N	2.039(3)	2.086(4)	2.0614(18)	2.170(3)	1.992(4)
			2.2592(16)	2.318(3)	2.070(3)
M-N_{BTD}	2.047(3)	-	2.0919(17)	2.183(3)	1.979(3)
τ_4/τ_5	0.93	0.90	0.107	0.086	0.003
angles (C1C6C8N3)	17.94	128.92	3.60	0.70	1.17
BVS	2.12[33,34]	1.92[34]	2.05[34]	2.01[33,35]	2.21[34,36]
M···M	6.3713(6)	7.7060(14)	7.6234(8)	7.7062(8)	7.3010(7)
π-π	3.83	3.39	3.36	3.6919	3.6599
				3.8599	3.7480
S···N	-	-	2.9793	3.068	2.9764
S···S	-	3.51	-	-	-

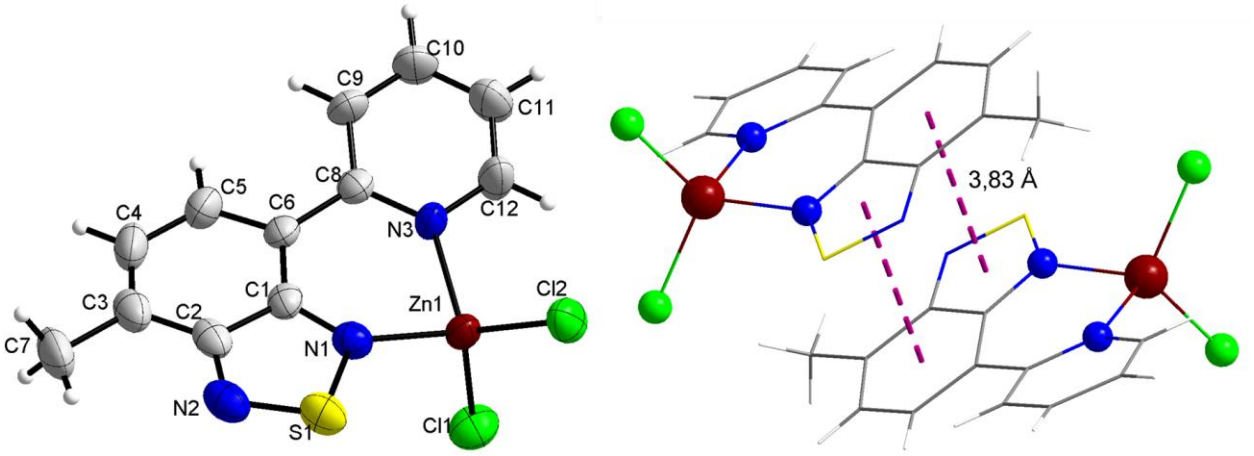

Figure 3. Views of the molecular structure of **1**, with the numbering scheme and displacement ellipsoids drawn at the 50% probability level (left), and its supramolecular dimer through π-π interactions (right).

The crystal packing the **1** shows the presence of π-π stacking and two types of weak intermolecular C–H···Cl type interactions (Table 3) that lead to the molecular assembling into a one-dimensional supramolecular structure (Figure S14, ESI†). The π-π stacking pattern between BTD units with centroid-centroid distances of 3.83 Å (Fig. 3) affords supramolecular dimers as repeating intrachain motifs (Figure S14, ESI†).

Table 3. Hydrogen bond parameters (Å, °) of complexes **1-5** (excluding solvent molecules)

C-H···Cl	d(H···Cl)	d(C···Cl)	angles (C-H···Cl)
	1		
C(7) – H(7B)···Cl(2)′	2.79	3.68	154
C(12) – H(12)···Cl(2)″	2.79	3.53	137
	2		
C(11) – H(11)···Cl(2)′	2.88	3.59	133
	3		
C(5)-H(4)···Cl(1)′	2.72	3.61	159
C(9)-H(14)···Cl(1)′	2.72	3.64	171
C(15)-H(22)···Cl(1)″	2.86	3.52	130
	4		
C(5)-H(5)···Cl(1)′	2.77	3.67	163
C(9)-H(9)···Cl(1)′	2.82	3.73	169
C(14)-H(14)···Cl(2)″	2.87	3.63	128

C(17)-H(17)···Cl(2)‴	2.95	3.66	134
	5		
C(5)-H(5)···Cl(1) ′	2.63	3.51	159
C(9)-H(9)···Cl(1) ′	2.78	3.70	170
C(15)-H(15) ··· Cl(1)″	2.65	3.49	130

L^1 exhibits a *trans* configuration in the case of **2** with a N3C8C6C1 torsion angle equal to 128.92° and the nitrogen BTD atoms are not involved in the coordination with the zinc atom (Fig. 4). This feature allows the BTD unit to be involved in a certain number of intermolecular interactions. Weak C-H···Cl type interactions connect the molecules of **1** along the crystallographic *a* axis leading to supramolecular chains which are interlinked by S···S intermolecular interactions, forming 2D supramolecular layers (Figure S15). These layers are further extended into a supramolecular 3D structure due to π-π stacking interactions between thiadiazole rings (3.39 Å) (Fig. 4).

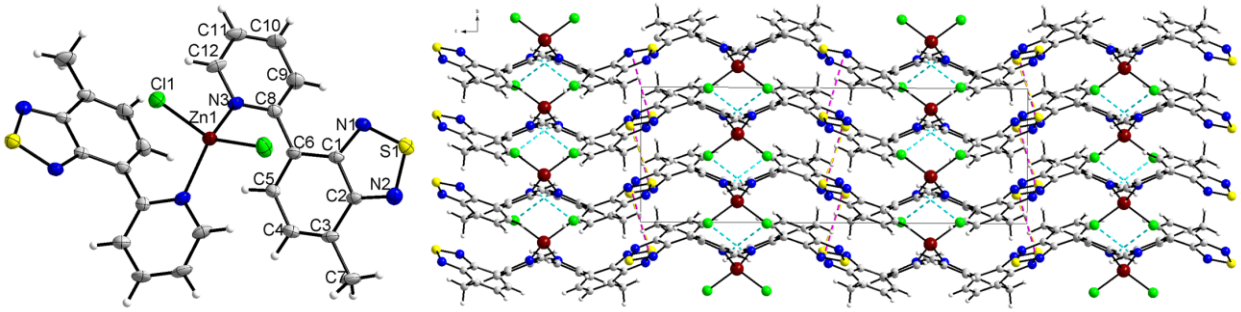

Figure 4. Views of the molecular structure of **2**, with the numbering scheme and displacement ellipsoids drawn at the 50% probability level (left), and its supramolecular 3D structure (right).

Complexes **3-5** are isostructural in spite of the absence (**3**) or presence of crystallization solvent molecules, i.e. CH_2Cl_2 (**4**) and H_2O (**5**). The metal ions in them are five-coordinate in a slightly distorted N_3Cl_2 square pyramidal geometry built by two chloride ions and one molecule of the tridentate (*N*,*N*,*N*) ligand. [Figs. 5 (**3**) and S16 ESI† (**4** and **5**), Tables 2 and S8-S10, ESI†). The largest deviation from this geometry is observed in the structure of **3** [τ_5 = 0.107],[37] while the smallest one occurs in the case of **5** [τ_5 = 0.003]. The N1N3N4Cl2 set of atoms define the basal plane of the pyramid and the Cl1 atom fills the apical position. The metal atom is displaced from the mean equatorial plane by 0.307 (Cu), 0.544 (Zn) and 0.629 Å (Mn).

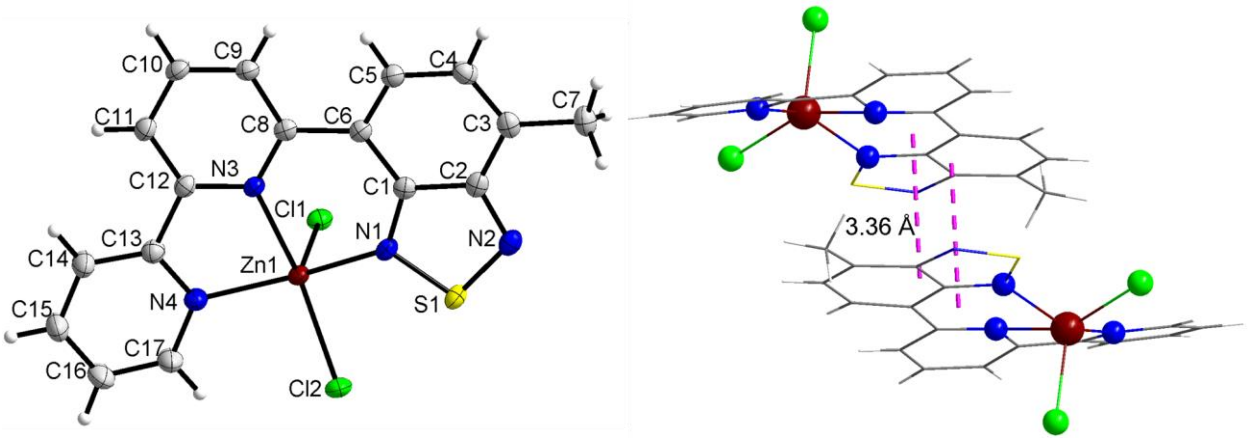

Figure 5. Views of the molecular structure of **3**, with the numbering scheme and displacement ellipsoids drawn at the 50% probability level (left), and its supramolecular dimer through π-π stacking (right).

In the crystal packing the molecules assemble through C-H···Cl hydrogen bond interactions (Table 3), π-π stacking and S···N interactions leading to 3D supramolecular structures (Fig. 6 for **4**, Figure S17 and S18 ESI† for **3** and **5**).

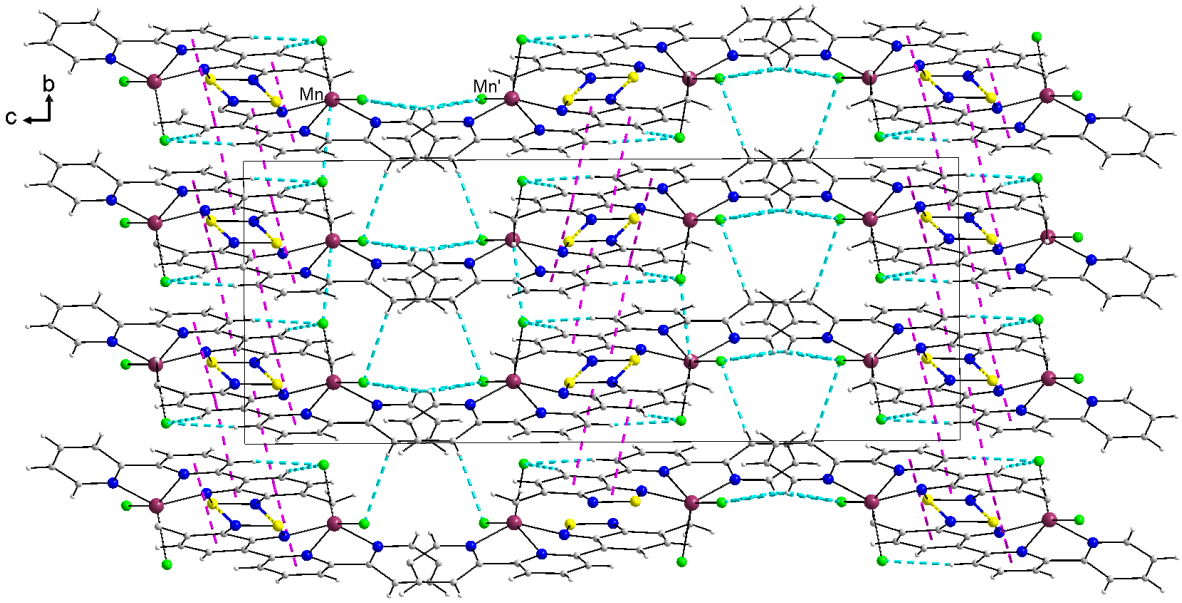

Figure 6. Crystal packing of **4** in the *bc* plane showing the various intermolecular interactions. Solvent molecules have been omitted for clarity.

Photophysical properties of L^1, L^2 and their Zn(II) complexes (1-3)

The absorption, emission and excitation spectra of L^1, L^2 and $[ZnL^1Cl_2]$ (**1**), $[Zn(L^1)_2Cl_2]$ (**2**) and $[ZnL^2Cl_2]$ (**3**) were measured in CH_2Cl_2 solutions ($c \approx 1 \cdot 10^{-5}$ M).

The UV-visible absorption spectra of L^1 and L^2 show three bands: the first one, which is located at 250 nm for L^1, is doubled for L^2 (240 and 263 nm); the second peak is splitted for the two ligands [306 and 318 nm (L^1), and 311 and 318 nm (L^2)]; the last intense peaks appear at 362 and 370 nm for L^1 and L^2, respectively (Fig. 7). Both ligands show luminescent behaviour with λ_{max} 460 and 462 nm for L^1 and L^2, respectively. Excitation and absorption spectra of the ligands are identical, confirming that the luminescence is clearly due to the compounds and not to some impurity or decomposition products.

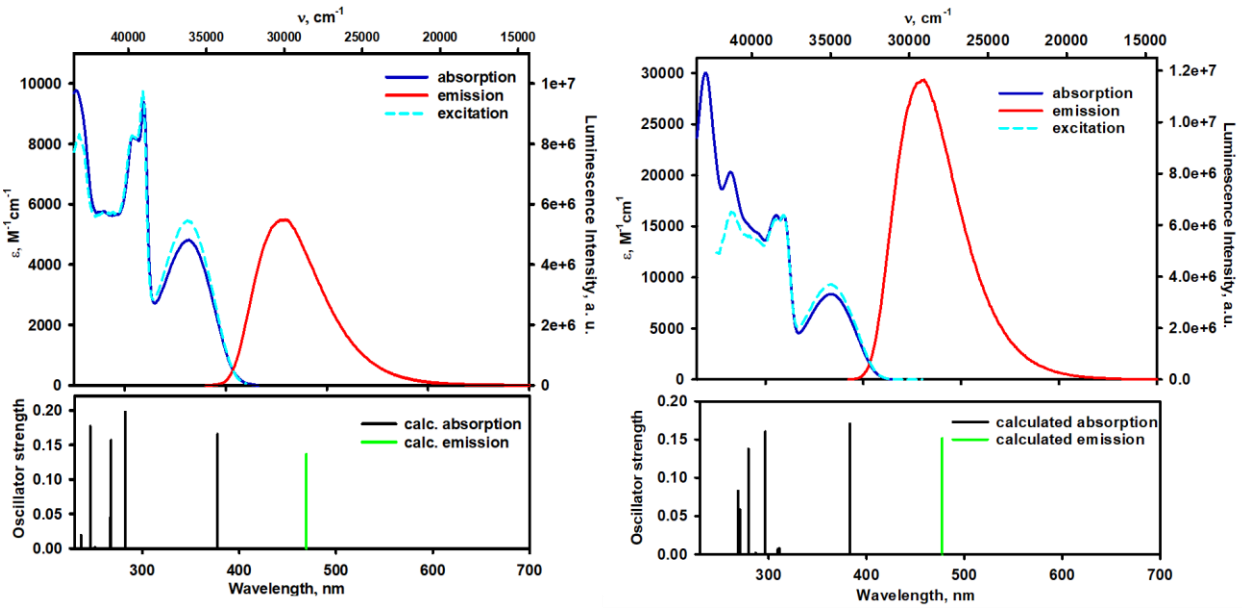

Figure 7. Comparison of the experimental (line graph) and calculated (stick plot) absorption, excitation and emission spectra of L^1 (left) and L^2 (right), (experimental spectra were measured in CH_2Cl_2, $c \approx 1 \cdot 10^{-5}$ M, $\lambda_{em} = 460$ nm, $\lambda_{ex} = 360$ nm and $\lambda_{em} = 470$ nm, $\lambda_{ex} = 375$ nm, respectively).

Time Dependent DFT (TD-DFT) calculations were performed to have an insight into the absorption and emission properties (see computational details). The experimental data will be compared with the calculated *trans*- forms of the ligands, due to their relative higher stability than the *cis*- forms. The simulated absorption and luminescence correlate well with the experimental ones (Fig. 7). Furthermore, with the TD-DFT results, one can represent the electron density difference (EDD) between the excited state and the ground state (Fig. 8). The experimental absorption band with a maximum at 362 nm corresponds to the calculated $S_0 \rightarrow S_1$ transition with a maximum at 377 nm. This transition can be attributed to a $\pi \rightarrow \pi^*$ transition, which is mainly the HOMO → LUMO excitation. The EDD of the $S_0 \rightarrow S_1$ transition clearly shows electron density

moving from benzene and pyridine rings to the thiadiazole part of the ligand (from donor to acceptor). The second absorption band combines three transitions with a large contribution of $S_0 \rightarrow S_3$ and $S_0 \rightarrow S_4$, which is mainly a py $\pi \rightarrow \pi^*$ transition. The third peak in the low-wavelengths region is dominated by $S_0 \rightarrow S_8$ and corresponds to a BTD $\pi \rightarrow \pi^*$ transition. The spectra of L^2 looks similar to the one of L^1 and it is mainly described by analogous transitions (Figure S19, ESI†). The calculated emission spectra have maxima at 469 and 477 nm for L^1 and L^2 respectively, correlating well with the experimental ones at 460 and 462 nm (Fig. 7).

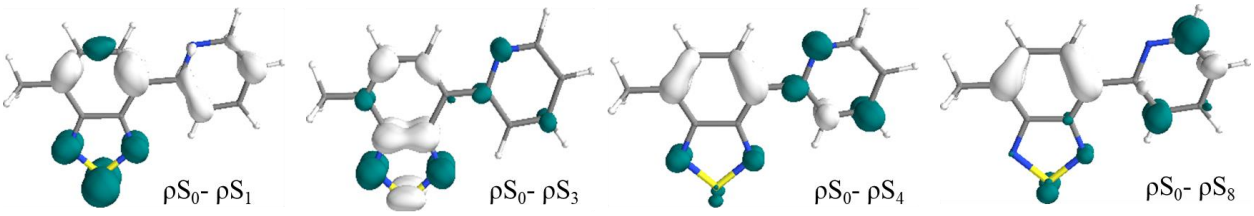

Figure 8. Density difference plots between the excited states and the ground state for L^1 (the excited electron and the hole regions are indicated by blue and white surfaces, respectively).

The normalized absorption and luminescence spectra of **1**-**3** in CH_2Cl_2 are shown in Fig. 9 together with those of the corresponding ligands for comparison. There is a slight bathochromic shift of the bands in the low-energy region of both the absorption and emission of **1**-**3** compared to the free ligands (see also Figures S20-S23) very likely because of the coordination of the thiadiazole unit.

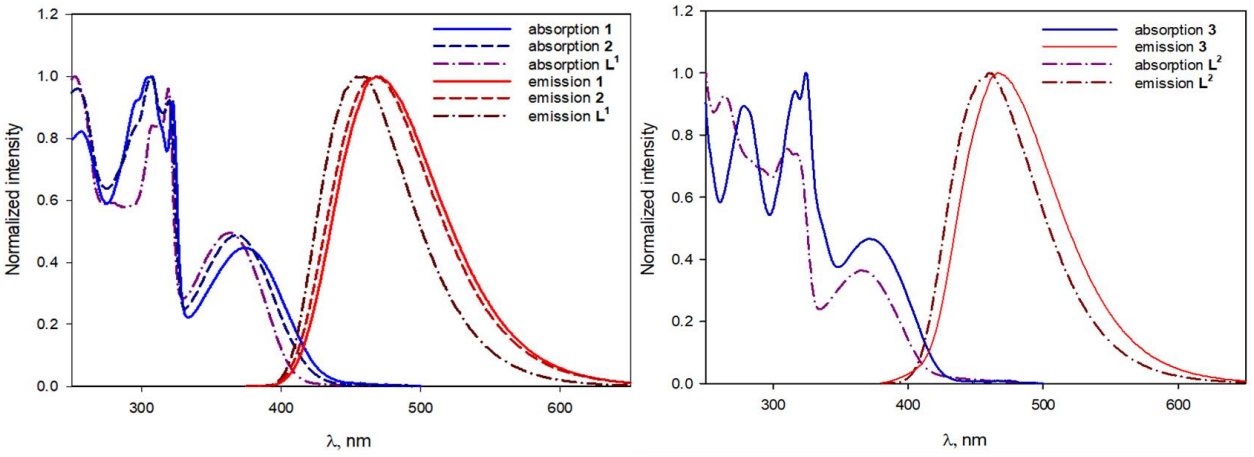

Figure 9. Normalized absorption and luminescence spectra in CH_2Cl_2 of **1, 2** and L^1 (left) and **3** and L^2 (right).

The solid-state luminescence of complexes **1** and **3** indicates red-shift of the emission bands compared to the free ligands (Fig. 10), similar to their behaviour in solution (see Fig. 9). In contrast, complex **2** displays a blue-shift of the emission in the solid-state compared to the free ligand L^1 (Fig. 10). This solid-state blue-shift of **2**, opposite to the one in solution, can probably be explained by the difference of coordination of L^1 to the metal ion between the solution and the solid-state. In the latter, the thiadiazole units, uncoordinated to the zinc(II) ion, stack on the top of each other as in the H-type aggregates (see Fig. 4 and S15), very likely inducing the observed blue-shift. On the contrary, in solution, the emission band of complex **2** appears at a similar wavelength (463 nm) to those of complexes **1** and **3**, i.e. 468 and 467 nm, yet the red-shift is smaller than for complex **1** containing the same ligand L^1, suggesting some weak coordination of the N thiadiazole atoms to the metal ion in **2**, unlike the solid-state situation.

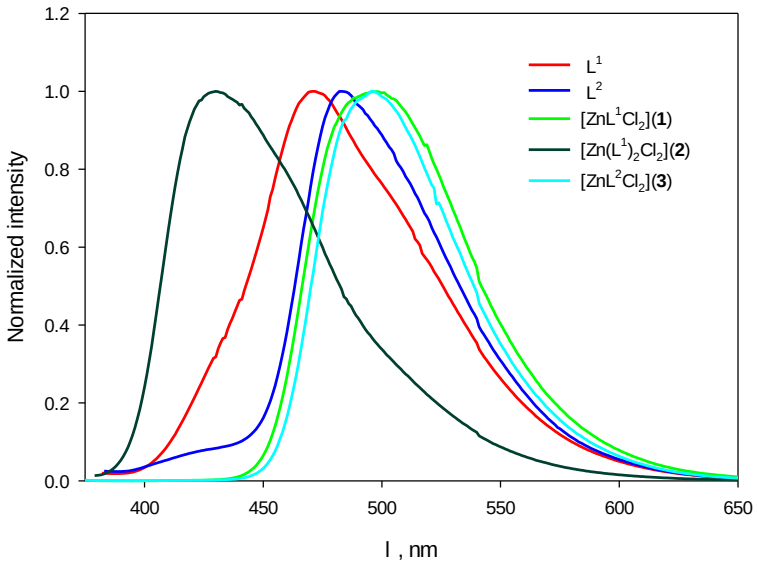

Figure 10. Normalized luminescence spectra of L^1, L^2, and **1-3**, in the solid-state at room temperature (λ_{ex} = 360 nm, λ_{max} = 471 nm (L^1), 483 nm (L^2), 496 nm (**1**), 430 nm (**2**), 496 nm (**3**)).

The luminescence quantum yields (η) were determined with diphenyl-anthracene as a standard reference with excitation at 360 nm having a luminescence quantum efficiency of 95% in *n*-heptane at room temperature, using the expression of eq.(1):

$$\eta = \frac{\int I_{lum}^{sample}(\lambda)d\lambda}{\int I_{lum}^{ref}(\lambda)d\lambda} \cdot \frac{OD_{\lambda ex}^{ref}}{OD_{\lambda ex}^{sample}} \cdot \left(\frac{n_{solv}^{sample}}{n_{solv}^{ref}}\right)^2 \quad (1)$$

where $\int I_{lum}^{sample}(\lambda)d\lambda$ and $\int I_{lum}^{sample}(\lambda)d\lambda$ are the integrated luminescence intensities from the spectra corrected for the spectral response of the system, $OD_{\lambda ex}^{ref}$ and $OD_{\lambda ex}^{sample}$ stand for the optical densities or absorbance at the excitation wavelength, and n_{solv}^{sample} and n_{solv}^{sample} correspond to the refractive indices of the solvents for the sample and the reference, respectively.

The luminescence quantum efficiencies of L^1, L^2, and **1-3** in solution are given in Table 4. The values both for ligands and complexes are relatively high, in line with the one reported for the ligand (2'-Py)$_2$BTD (Scheme 1).[28]

Table 4. Luminescence quantum efficiencies (η, %) of L^1, L^2, **1**, **2** and **3** in CH_2Cl_2 solutions at room temperature

	L^1	L^2	**1**	**2**	**3**
η, %	76	74	61	87	91

Magnetic properties of $[MnL^2Cl_2]\cdot 0.5CH_2Cl_2$ (4) and $[CuL^2Cl_2]\cdot H_2O$ (5)

The magnetic properties of **4** and **5** under the form of $\chi_M T$ against T plots [χ_M is the magnetic susceptibility per one Mn(II) (**4**) or one Cu(II) (**5**) ions] are shown in Fig. 11. The values of $\chi_M T$ at room temperature are 4.38 (**4**) and 0.41 cm^3 mol^{-1} K (**5**). They are as expected for one magnetically non-interacting spin sextuplet ($\chi_M T$ = 4.735 cm^3 mol^{-1} K with S_{Mn} = 5/2 and g_{Mn} = 2.0) or doublet ($\chi_M T$ = 0.41 cm^3 mol^{-1} K with S_{Cu} = ½ and g_{Cu} = 2.10) local spins. Upon cooling down, these values remain constant until ca. 50 K and they further decrease to 3.07 (**4**) and 0.17 cm^3 mol^{-1} K (**5**) at 2.0 K. Weak intermolecular antiferromagnetic interactions would account for the decrease of $\chi_M T$ in both compounds.

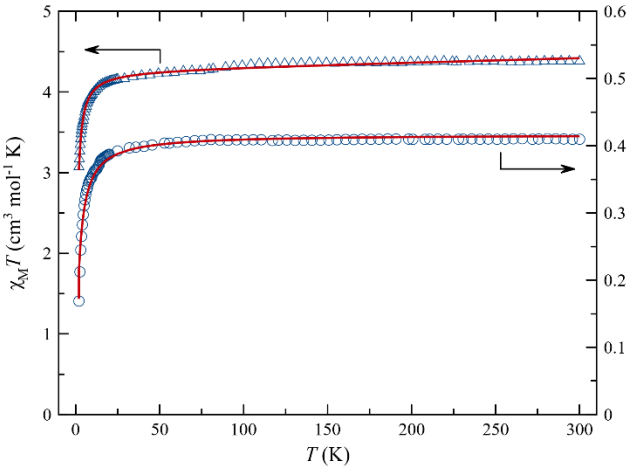

Figure 11. Temperature dependence of the $\chi_M T$ product for **4** (Δ) and **5** (o). The solid lines are the best-fit curves through eq (2) (see text).

Having in mind the mononuclear nature of **4** and **5** and the above considerations, their magnetic data were treated through a Curie law for a manganese(II) (S = 5/2) or a copper(II) ion (S = ½) [eq (2)]

$$\chi_M = N\beta^2 g^2 (S(S+1)/3k(T-\theta) \qquad (2)$$

where N, β and k have their usual meanings and θ is a Curie-Weiss term that was introduced to take into account the intermolecular magnetic interactions. Least-squares best fit parameters are g = 2.00(1) and θ = -0.78(1) K for **4** and g = 2.09(1) and θ = -2.09(1) K for **5**. The different weak intermolecular interactions (C-H···Cl contacts, π-π stacking and S···N interactions; see Figs. 6 and S17 and Tables 2 and 3) would provide the exchange pathways, the small magnetic interactions being in line with the great values of the shortest intermolecular metal-metal separations [7.7062(8) Å for Mn···Mn^I and 7.3010(7) Å for Cu···Cu^I; symmetry code: (I) = 1-x, y, 0.5-z (**4**) and (I) = 1-x, 1-y, 1-z (**5**)].

Conclusions

Highly fluorescent chelating bidentate 1,3,2-benzothiadiazole-pyridine (L^1) and tridentate -2,2'-bipyridine (L^2) ligands have been synthesized and fully characterized. Depending on the reaction conditions with $ZnCl_2$, L^1 provided either the tetrahedral complex **1**, where the metal ion is chelated by the pyridyl and thiadiazole nitrogen atoms, or the tetrahedral complex **2** containing

two L^1 molecules acting as monodentate ligands through the pyridyl nitrogen atom, while L^2 afforded only complex **3** in which the ligand is tridentate and the metal ion is five-coordinate in a square pyramidal geometry. A complex set of non-covalent intermolecular interactions such as π-π stacking, C-H···Cl type, S···S and N···S short contacts are observed in the solid state supramolecular structures. The three complexes are highly fluorescent, with values of the quantum yields in solution of 61-91%, and showing a bathochromic shift of the emission compared to the free ligands. In the solid state the emission properties of the complexes show interesting trends. While complexes **1** and **3** show a red-shift compared to the free ligand, complex **2** shows a blue-shift. This feature can be explained by the different coordination of the zinc(II) ion by the two ligands L^1 in solution and in the solid-state, together with supramolecular interactions established in the solid-state. These results provide valuable insight into the relationship between ligand coordination, aggregation and emission properties. The paramagnetic mononuclear compounds **4** and **5** were obtained with $MnCl_2$ and $CuCl_2$ salts respectively. The metal ions in them exhibit square pyramidal surroundings and their magnetic properties reveal a Curie-Weiss behaviour corresponding to weak intermolecular antiferromagnetic interactions. These results demonstrate the interest and modularity of the new BTD based ligands towards luminescent and magnetically active complexes and further work will be devoted to the coordination of other metal centres, including lanthanides in order to access to such functional complexes.

Experimental section

General procedures

Starting chemicals were purchased from commercial sources and used as received. All the reactions were carried out under ambient conditions (unless otherwise indicated) with HPLC-grade solvents. Nuclear magnetic resonance spectra were recorded on a Bruker Avance DRX 300 spectrometer operating at 300 and 75 MHz for ^1H and ^{13}C, respectively. Chemical shifts are expressed in ppm downfield from external TMS. The following abbreviations (δ) are used: s, singlet; d, doublet; t, triplet; m, multiplet. MALDI-TOF MS spectra were done on a Bruker Biflex-IIITM apparatus, equipped with a 337 nm N_2 laser. ESI-MS spectra were achieved on a Bruker MicrO-Tof-Q 2 spectrometer. Elemental analyses (C, H, N and S) were recorded using a Flash 2000 Fisher Scientific Thermo Electron analyzer. The IR spectra were taken on an ATR Bruker Vertex 70 spectrophotometer in the range 4000-400 cm^{-1} (at 1 cm^{-1} resolution). Signal intensities

(height) are denoted by the following abbreviations: vs-very strong, s-strong, m-medium and w-weak. UV-Vis absorption spectra of the compounds in dichloromethane were measured on a Cary 5000 (Agilent) spectrophotometer. Emission and excitation spectra likewise were recorded on a Fluorolog 3 (Horiba-Jobin-Yvon) spectrophotometer and corrected for the spectral response of the apparatus. The emission and excitation spectra in the solid state were measured using a Jasco FP-8500 spectrofluorimeter. Cyclic voltammetry (CV) measurements were performed inside a glove box, by using a three-electrode cell that was equipped with Ag wire pseudo-reference electrode, Pt working electrode, and Pt counter electrode. Ferrocene was used as an internal reference and then the Fc/Fc+ couple values have been adjusted to zero. The potentials were re-adjusted with respect to the saturated calomel electrode (SCE). The electrolyte was a 0.1 mol L^{-1} solution of *n*-Bu_4NPF_6 in DCM. All of the experiments were performed at RT at a scan rate of 100 mV/s. The voltammograms were recorded on a BioLogic SP-150 potentiostat.

Synthesis

4-(2'-pyridyl)-7-methyl-2,1,3-benzothiadiazole (L^1). 4-Methyl-7-(4,4,5,5-tetramethyl-1, 3,2-dioxaborolan-2-yl)-2,1,3-benzothiadiazole **I** (600 mg, 2.17 mmol), 2-bromopyridine (0.21 mL, 2.17 mmol) and tetrakis(triphenylphosphine)palladium [$Pd(PPh_3)_4$] (109 mg, 108.63 μmol) were dissolved in degased toluene (7 mL). The resulting mixture was evacuated and backfilled with argon in Schlenk flask. Potassium carbonate solution (1.8 g, 13.04 mmol in 1.8 mL water) was added and the solution was stirred at 80 °C for 48 h. After cooling, the solvent was removed under vacuum and the residue diluted with water and dichloromethane. The organic layer was separated, washed with water, brine and dried over $MgSO_4$. The solvent was evaporated under reduced pressure. The compound was purified by column chromatography (SiO_2, CH_2Cl_2/EtOAc = 10:0 → 9:1 v/v) to give a white solid. Yield: 286 mg (58.0 %). Elemental analysis calcd. (%) for $C_{12}H_9N_3S$: C, 63.74; H, 3.99; N, 18.49; S, 14.11. Found: C, 63.45; H, 3.94; N, 17.99; S, 13.73. IR (ATR, ν_{max} cm^{-1}): 2918w, 1738w, 1581s, 1548s, 1462s, 1433s, 1374s, 1324m, 1266s, 1095m, 1068s, 1050m, 992s, 947s, 884s, 861s, 844s, 795s, 772vs, 739s, 728s, 624s, 557s, 536s, 508s, 497s. Exact mass: 226.0449, 227.0516. ^1H NMR (300 MHz, $CDCl_3$) δ 8.77 (s, 1H), 8.61 (d, J = 7.8 Hz, 1H), 8.34 (d, J = 6.9 Hz, 1H), 7.85 (t, J = 7.6 Hz, 1H), 7.52 (d, J = 6.6 Hz, 1H),), 7.36-7.31 (m),, 2.80 (s, 3H). ^{13}C NMR (76 MHz, $CDCl_3$) δ 156.34, 154.55, 153.06, 149.80, 136.68, 132.59, 129.82, 129.68, 128.68, 124.74, 122.83, 18.37.

4-[6'-(2,2′-bipyridyl)]-7-methyl-2,1,3-benzothiadiazole (L^2). 4-Methyl-7-(4,4,5,5-tetramethyl-1,3,2-dioxaborolan-2-yl)-2,1,3-benzothiadiazole **I** (530 mg, 1.92 mmol), 6-bromo-2,2′-bipyridine (451 mg, 1.92 mmol) and tetrakis(triphenylphosphine)palladium [$Pd(PPh_3)_4$] (111 mg, 95.96 μmol) were dissolved in degased toluene (7 mL). The resulting mixture was evacuated and backfilled with argon in Schlenk flask. Potassium carbonate solution (1.59 g, 11.51 mmol in 1.7 mL water) was added and the solution was stirred at 80 °C for 48 h. After cooling, the solvent was removed under vacuum and the residue diluted with water and dichloromethane. The organic layer was separated, washed with water, brine and dried over $MgSO_4$. The solvent was evaporated under reduced pressure. The compound was purified by column chromatography (SiO_2, CH_2Cl_2/EtOAc = 10:0 → 9:1 v/v) to give a white solid. Yield: 300 mg (51.5 %). Elemental analysis calcd. (%) for $C_{17}H_{12}N_4S$: C, 67.08; H, 3.97; N, 18.41; S, 10.53. Found: C, 66.78; H, 3.94; N, 18.31; S, 10.50. IR (ATR, ν_{max} cm^{-1}): 2917w, 1578s, 1549s, 1492s, 1472m, 1455s, 1429s, 1370m, 1310m, 1277m, 1255s, 1169m, 1088s, 1044s, 993s, 965m, 892s, 865m, 850s, 825s, 793s, 773vs, 744s, 700s, 635s, 618s, 587s, 540s, 499s, 471m, 421m. Exact mass, m/z 303.0710, 304.0784. ^{1}H NMR (300 MHz, $CDCl_3$) δ 8.78 (d, J = 7.3 Hz, 1H), 8.72 (d, J = 4.5 Hz, 1H), 8.63 (t, J = 7.5 Hz, 2H), 8.44 (d, J = 7.8 Hz, 1H), 8.00 (t, J = 7.9 Hz, 1H), 7.87 (td, J = 7.7, 1.7 Hz, 1H), 7.56 (dd, J = 7.2, 1.0 Hz, 1H), 7.34 (ddd, J = 7.4, 4.8, 1.0 Hz, 1H), 2.83 (s, 3H). ^{13}C NMR (76 MHz, $CDCl_3$) δ 156.39, 156.30, 155.74, 153.36, 153.09, 149.17, 137.57, 136.91, 132.52, 129.64, 128.54, 124.60, 123.79, 121.28, 120.00, 18.14.

[ZnL^1Cl_2] (1). To a light-yellow solution of L^1 (20 mg, 0.088 mmol) in DCM (3 mL), was added a solution of zinc(II) chloride (24 mg, 0.176 mmol) in methanol (3 mL). The reaction mixture was magnetically stirred at 25°C for 5 hours. After 7 days of slow evaporation, yellow crystals were collected by filtration. Yield: 24 mg (37.8 %). Anal. calcd. for $C_{12}H_9Cl_2N_3SZn$ (%): C, 39.64; H, 2.50; N, 11.56; S, 8.82. Found (%): C, 36.73; H, 2.65; N, 11.02; S, 8.65. IR (ATR, ν_{max} cm^{-1}): 3084w, 1600s, 1552s, 1481vs, 1432s, 1368m, 1294s, 1274m, 1246m, 1216m, 1164s, 1102m, 1061s, 1028s, 910vs, 877s, 866s, 793vs, 774vs, 742m, 724s, 668m, 650m, 617m, 557s, 545s, 515s, 506s, 464m, 415m. MALDI-TOF MS (m/z): 326 $[ZnL^1Cl]^+$. ^{1}H NMR (300 MHz, $CDCl_3$) δ 9.05 (d, *J* = 6.2 Hz, 1H), 8.43 (d, *J* = 7.5 Hz, 1H), 8.29 (d, *J* = 8.4 Hz, 1H), 8.21 – 8.11 (m, 1H), 7.72 (dd, *J* = 7.8, 1.5 Hz, 1H), 7.67 (d, *J* = 6.5 Hz, 1H), 2.90 (d, *J* = 1.1 Hz, 3H). ^{1}H NMR (300 MHz, CD_2Cl_2) δ 8.97 (ddd, *J* = 5.4, 1.8, 0.9 Hz, 1H), 8.48 (d, *J* = 7.5 Hz, 1H), 8.33 (d, *J* =

8.4 Hz, 1H), 8.21 (ddd, *J* = 8.4, 7.5, 1.8 Hz, 1H), 7.79 – 7.72 (m, 1H), 7.69 (ddd, *J* = 7.5, 5.4, 1.2 Hz, 1H), 2.89 (d, *J* = 1.1 Hz, 3H).

[Zn(L^1)$_2$Cl$_2$] (2). To a light-yellow solution of L^1 (20 mg, 0.088 mmol) in DCM (3 mL), was added a solution of zinc(II) chloride (12 mg, 0.088 mmol) in methanol (3 mL). The reaction mixture was magnetically stirred at 65 °C for 2 hours. After 1-3 days of slow evaporation, colorless crystals were collected by filtration. Yield: 26 mg (49.9 %). Anal. calcd. for $C_{24}H_{18}Cl_2N_6S_2Zn$ (%): C, 48.79; H, 3.07; N, 14.22; S, 10.85. Found (%): C, 48.05; H, 2.99; N, 10.83; S, 10.75. IR (ATR, ν_{max} cm^{-1}): 3075w, 1609m, 1590m, 1559s, 1477s, 1435s,1378m, 1343m, 1289m, 1268m, 1237m, 1160m, 1103m, 1077s, 1057m,1019m, 951m,923m, 883s, 848s, 827vs, 792s, 776vs, 766s, 755s, 729m, 649m, 637m, 621s, 557s, 549s, 508s, 463m, 420s. ESI-MS (m/z): 553.05 [Zn(L^1)$_2$Cl]$^+$. ^{1}H NMR (300 MHz, $CDCl_3$) δ 8.89 (d, J = 5.1 Hz, 1H), 8.48 (d, J = 8.1 Hz, 1H), 8.39 (d, J = 7.3 Hz, 1H), 8.04 – 7.94 (m, 1H), 7.62 (dd, J = 7.4, 1.3 Hz, 1H), 7.50 – 7.42 (m, 1H), 2.85 (d, J = 1.1 Hz, 3H).^{1}H NMR (300 MHz, CD_2Cl_2) δ 8.85 (ddd, J = 5.1, 1.9, 0.9 Hz, 1H), 8.53 (dt, J = 8.2, 1.1 Hz, 1H), 8.45 (d, J = 7.4 Hz, 1H), 8.03 (ddd, J = 8.2, 7.6, 1.9 Hz, 1H), 7.65 (dq, J = 7.4, 1.1 Hz, 1H), 7.50 (ddd, J = 7.6, 5.1, 1.1 Hz, 1H), 2.84 (d, J = 1.1 Hz, 3H).

[ZnL^{2}Cl$_2$] (3). To a light-yellow solution of L^2 (20 mg, 0.066 mmol) in DCM (3 mL), was added a solution of zinc(II) chloride (9 mg, 0.066 mmol) in methanol (3 mL). The reaction mixture was magnetically stirred at 65 °C for 2 hours. After 1-3 days of slow evaporation, yellow crystals were collected by filtration. Yield: 14 mg (47.8 %). Anal. calcd. for $C_{17}H_{12}Cl_2N_4SZn$ (%): C, 46.34; H, 2.74; N, 12.71; S, 7.28. Found (%): C, 44.96; H, 2.63; N, 11.87; S, 7.17. IR (ATR, ν_{max} cm^{-1}): 3083w, 1595s, 1569s, 1553s, 1486s, 1448vs, 1402s, 1296s, 1266m, 1235s, 1217s, 1193s, 1158s, 1119s, 1073m, 1052s, 1025s, 997s, 954m, 929m, 914m, 892vs, 870s, 849s, 826s, 793vs, 736s, 705s, 645s, 626s, 586s, 564m, 549s, 515s, 502m, 483m, 456m, 427s, 412m. ESI-MS (m/z): 402.8 [ZnL^{2}Cl]$^+$. ^{1}H NMR (300 MHz, $CDCl_3$) δ 9.50 (d, J = 5.4 Hz, 1H), 8.41 – 8.06 (m, 6H), 7.75 (s, 1H), 7.63 (d, J = 8.3 Hz, 1H), 2.87 (s, 3H).

[MnL^2(Cl)$_2$]·0.5CH$_2$Cl$_2$ (4). To a light-yellow solution of L^2 (20 mg, 0.066 mmol) in DCM (3 mL), was added a solution of manganese(II) chloride tetrahydrate (13 mg, 0.066 mmol) in methanol (3 mL). The reaction mixture was magnetically stirred at 65 °C for 2 hours. After 1-3 days of slow evaporation, pink crystals were collected by filtration. Yield: 20 mg (64.5 %). Anal.

calcd. for $C_{18}H_{14}Cl_4N_4SMn$ (%): C, 41.97; H, 2.74; N, 10.88; S, 6.22. Found (%): C, 45.11; H, 2.86; N, 12.31; S, 6.78. IR (ATR, ν_{max} cm^{-1}): 3324w, 2973m, 2886w, 1594s, 1555s, 1550s, 1484s, 1444vs, 1398s, 1297s, 1263m, 1230s, 1213s, 1157m, 1117m, 1087s, 1047vs, 995m, 888vs, 866s, 853m, 826s, 792vs, 782s, 734s, 704s, 644s, 625s, 586s, 564m, 549s, 515s, 502m, 483m, 451m, 421m, 411m. ESI-MS (m/z): 393.9 $[MnL^9Cl]^+$.

$[CuL^2Cl_2]\cdot H_2O$ (5). To a light-yellow solution of L^2 (20 mg, 0.066 mmol) in DCM (3 mL), was added a solution of copper(II) chloride dihydrate (11 mg, 0.066 mmol) in methanol (3 mL). The reaction mixture was magnetically stirred at 65 °C for 2 hours. After 1-3 days of slow evaporation, green crystals were collected by filtration. Yield: 19 mg (64.4 %). Anal. calcd. for $C_{17}H_{14}Cl_2N_4SOCu$ (%): C, 44.70; H, 3.09; N, 12.26; S, 7.02. Found (%): C, 44.90; H, 2.88; N, 12.80; S, 6.71. IR (ATR, ν_{max} cm^{-1}): 3034w, 1597s, 1552s, 1486s, 1448s, 1401s, 1304m, 1290m, 1235s, 1222s, 1189s, 1157s, 1119s, 1091m, 1075s, 1054m, 1028m, 1004s, 898m, 877s, 852s, 828m, 795s, 736vs, 706s, 657s, 645s, 630s, 584s, 565m, 553s, 521s, 501m, 482m, 460m, 434s, 416m. ESI-MS (m/z): 367.0$[CuL^9]^{2+}$, 402.0 $[CuL^9Cl]^+$.

Crystal structure determinations

Single crystals of the compounds were mounted on glass fibre loops using a viscous hydrocarbon oil to coat the crystal and then transferred directly to a cold nitrogen stream for data collection. Data collections were mostly performed on an Agilent Technologies SuperNova diffractometer equipped with an Atlas CCD detector and micro-focus Cu-Kα radiation (λ = 1.54184Å). The structures were solved by direct methods SHELXS-97[38] and refined on F^2 by full matrix least-squares techniques using the SHELX97 program[39] within WINGX.[40] All non-H atoms were refined anisotropically and multiscan empirical absorption was applied using the CrysAlisPro program (CrysAlisPro, AgilentTechnologies, V 1.171.41.118a, 2021). The hydrogen atoms were introduced at calculated positions (riding model) and included in structure factor calculations but not refined. Details about data collection and solution refinement are given in Tables S2 and S5. Supplementary crystallographic Figures S13-S18 and Tables S3-S4 and S6-S10 are reported in the ESI.

Crystallographic data for the seven structures have been deposited with the Cambridge Crystallographic Data Centre, deposition numbers CCDC 2277636 (L^1), CCDC 2277637 (L^2), CCDC 2277638 (**1**), CCDC 2277639 (**2**) , CCDC 2277640 (**3**), CCDC 2277641 (**4**) and CCDC

2277642 (**5**). These data can be obtained free of charge from CCDC, 12 Union road, Cambridge CB2 1EZ, UK (e-mail: deposit@ccdc.cam.ac.uk or http://www.ccdc.cam.ac.uk).

Computational details

Theoretical calculations have been performed using the Gaussian 09 package,[41] with the PBE0 hybrid functional[42] (with 25% of exact exchange) and 6-311++G(2df, 2pd) basis sets.[43,44] Optimized geometries were then confirmed as global minima by frequency calculations. For the calculations of the excited states, a Time Dependent DFT methodology has been employed with the same parameters as for the ground states. The first 10 to 20 singlets and 10 triplets have been calculated. The pictures of the molecular orbitals, molecular electrostatic potentials and electron density difference plots (between ground and excited state) have been generated by quchemreport, a homemade python program based on cclib that automate the quality control and report generation.[45,46] More details and supplementary theoretical Figures S24-S53 and Tables S11-S34 are reported in the ESI.

Magnetic measurements

Variable-temperature direct current (dc) magnetic susceptibility measurements (2.0–300 K) under applied dc magnetic fields of 5000 G ($T \geq 50$ K) and 100 G ($T < 50$ K) on crushed crystals of **4** and **5** were carried out with a Quantum Design SQUID magnetometer. The magnetic susceptibility data of these compounds were corrected for the diamagnetism of the constituent atoms and the sample holder (a plastic bag).

Associated content

Supporting information

The Supporting Information is available free of charge on the ACS Publications website at DOI:xxx, which include: NMR spectra of ligands and complex **1-3** ; CV curves; crystallographic data; absorption, excitation and emission spectra, DFT and TD-DFT calculations details.

Author information

ORCID

Nataliya Plyuta: 0000-0002-1835-5956

Thomas Cauchy: 0000-0003-4259-3257
Miguel Julve: 0000-0001-9006-8268
Narcis Avarvari: 0000-0001-9970-4494

Notes

The authors declare no competing financial interest.

Acknowledgements

This work was supported in France by the CNRS, the University of Angers, the ANR Pause Ukraine and the French Embassy in Kyiv (grant to N.P.). Financial support in Spain from the Ministerio Español de Ciencia, Innovación y Universidades (Project PID2019-109735GB-I00 and Unidad de Excelencia María de Maetzu CEX2019-000919) and the Generalitat Valenciana (Project AICO/2020/183) is gratefully acknowledged. The authors warmly acknowledge Prof. Andreas Hauser (University of Geneva, Switzerland) for preliminary spectroscopic investigations.

Keywords

Benzothiadiazole • Nitrogen Ligands • Crystal Structure Determination • DFT Calculations • Photophysical Properties

Notes and references

[1] K. R. J. Thomas, J. T. Lin, M. Velusamy, Y.-T. Tao, C.-H. Chuen, *Adv. Funct. Mater.* **2004**, *14*, 83–90.

[2] S. David, H.-J. Chang, C. Lopes, C. Brännlund, B. Le Guennic, G. Berginc, E. Van Stryland, M. V. Bondar, D. Hagan, D. Jacquemin, C. Andraud, O. Maury, *Chem. Eur. J.* **2021**, *27*, 3517–3525.

[3] T. S. Sukhikh, D. S. Ogienko, D. A. Bashirov, S. N. Konchenkoa, *Russ. Chem. Bull.* **2019**, *68*, 651–661.

[4] C. T. Chen, *Chem. Mater.* **2004**, *16*, 4389–4400.

[5] B. A. D. Neto, A. A. M. Lapis, E. N. da Silva Júnior, J. Dupont, *Eur. J. Org. Chem*. **2013**, 228–255.

[6] M. Zhang, H. N. Tsao, W. Pisula, C. Yang, A. K. Mishra, K. Müllen, *J. Am. Chem. Soc.* **2007**, *129*, 3472–3473.

[7] L.-Y. Lin, Y.-H. Chen, Z.-Y. Huang, H.-W. Lin, S.-H. Chou, F. Lin, C.-W. Chen, Y.-H. Liu, K.-T. Wong, *J. Am. Chem. Soc.* **2011**, *133*, 15822–15825.

[8] Y. Geng, F. Pop, C. Yi, N. Avarvari, M. Grätzel, S. Decurtins, S.-X. Liu, *New J. Chem.* **2014**, *38*, 3269–3274.

[9] J. Du, M. C. Biewer, M. C. Stefan, *J. Mater. Chem. A* **2016**, *4*, 15771–15787.

[10] M. Li, C. An, W. Pisula, K. Müllen, *Acc. Chem. Res.* **2018**, *51*, 1196–1205.

[11] F. Pop, A. Amacher, N. Avarvari, J. Ding, L. M. Lawson Daku, A. Hauser, M. Koch, J. Hauser, S.-X. Liu, S. Decurtins, *Chem. Eur. J.* **2013**, *19*, 2504–2514.

[12] F. Pop, S. Seifert, J. Hankache, J. Ding, A. Hauser, N. Avarvari, *Org. Biomol. Chem.* **2015**, *13*, 1040–1047.

[13] M. R. Ams, N. Trapp, A. Schwab, J. V. Milić, F. Diederich, *Chem. Eur. J.* **2019**, *25*, 323–333.

[14] N. Biot, D. Bonifazi, *Coord. Chem. Rev.* **2020**, *413*, 213243.

[15] P. B. Pati, *Asian J. Org. Chem.* **2023**, e202300056.

[16] N. W. Alcock, A. F. Hill, M. S. Roe, *J. Chem. Soc. Dalton Trans.* **1990**, *5*, 1737–1740.

[17] S. Dey, A. S. Hazari, S. M. Mobin, G. K. Lahiri, *Dalton Trans.* **2022**, *51*, 8657–8670.

[18] G. S. Papaefstathiou, A. Tsohos, C. P. Raptopoulou, A. Terzis, V. Psycharis, D. Gatteschi, S. P. Perlepes, *Cryst. Growth Des.* **2001**, *1*, 191–194.

[19] M. Munakata, T. Kuroda-Sowa, M. Maekawa, M. Nakamura, S. Akiyama, S. Kitagawa, *Inorg. Chem.* **1994**, *33*, 1284–1291.

[20] M. W. Renner, K. M. Barkigia, D. Melamed, K. M. Smith, J. Fajer, *Inorg. Chem.* **1996**, *35*, 5120–5121.

[21] A. Pinto, M. Echeverri, B. Gómez-Lor, L. Rodríguez, *Dalton Trans.* **2022**, *51*, 8340–8349.

[22] D. A. Bashirov, T. S. Sukhikh, N. V. Kuratieva, D. Yu. Naumov, S. N. Konchenko, N. A. Semenov, A. V. Zibarev, *Polyhedron* **2012**, *42*, 168–174.

[23] F. S. Mancilha, L. Barloy, F. S. Rodembusch, J. Dupont, M. Pfeffer, *Dalton Trans.* **2011**, *40*, 10535–10544.

[24] X. Han, Q. Cheng, X. Meng, Z. Shao, K. Ma, D. Wei, J. Ding, H. Hou, *Chem. Commun.* **2017**, *53*, 10314–10317.

[25] T. S. Sukhikh, D. A. Bashirov, N. V. Kuratieva, A. I. Smolentsev, A. S. Bogomyakov, V. A. Burilov, A. R. Mustafina, A. V. Zibarev, S. N. Konchenko, *Dalton Trans.* **2015**, *44*, 5727–5734.

[26] N. Plyuta, T. Cauchy, A. Hauser, F. Lloret, M. Julve, N. Avarvari, *Polyhedron* **2022**, *224*, 115994.

[27] N. Plyuta, S. Petrusenko, V. N. Kokozay, T. Cauchy, F. Lloret, M. Julve, J. Cano, N. Avarvari, *Dalton Trans.* **2022**, *51*, 4760–4771.

[28] Md. Akhtaruzzaman, M. Tomura, J. Nishida, Y. Yamashita, *J. Org. Chem*. **2004**, *69*, 2953–2958.

[29] T. Mocanu, N. Plyuta, T. Cauchy, M. Andruh, N. Avarvari, *Chemistry* **2021**, *3*, 269–287.

[30] R. Agneeswari, V. Tamilavan, M. Song, M. H. Hyun, *J. Mater. Chem. C* **2014**, *2*, 8515–8524.

[31] T. Yamamoto, R. Murakami, M. Suginome *J. Am. Chem. Soc.* **2017**, *139*, 2557–2560.

[32] L. Yang, D. R. Powell, R. P. Houser *Dalton Trans.* **2007**, 955–964.

[33] I. D. Brown, D. Altermatt *Acta Crystallogr. B*, **1985**, *41*, 244–247.

[34] N. E. Brese, M. O'Keeffe *Acta Crystallogr. Sect. B* **1991**, *47*, 192–197.

[35] (IUCr) Bond valence parameters. https://www.iucr.org/resources/data/datasets/bond-valence-parameters.

[36] W. Liu, H. H. Thorp, *Inorg. Chem*. **1993**, *32*, 4102–4105.

[37] A. W. Addison, T. N. Rao, J. Reedijk, J. van Rijn, G. C. Verschoor, *J. Chem. Soc. Dalton Trans.* **1984**, 1349–1356.

[38] G. M. Sheldrick, *SHELX-97, Program for Crystal Structure Refinement*; University of Göttingen: Göttingen, Germany 1997.

[39] G. M. Sheldrick, *Acta Crystallogr. Sect. C Struct. Chem.* **2015**, *71*, 3–8.

[40] L. J. Farrugia, *J. Appl. Crystallogr*. **2012**, *45*, 849–854.

[41] M. J. Frisch, G. W. Trucks, H. B. Schlegel, G. E. Scuseria, M. A. Robb, J. R. Cheeseman, G. Scalmani, V. Barone, G. A. Petersson, H. Nakatsuji, X. Li, M. Caricato, A. Marenich, J. Bloino, B. G. Janesko, R. Gomperts, B. Mennucci, H. P. Hratchian, J. V. Ortiz, A. F. Izmaylov, J. L. Sonnenberg, D. Williams-Young, F. Ding, F. Lipparini, F. Egidi, J. Goings, B. Peng, A. Petrone, T. Henderson, D. Ranasinghe, V. G. Zakrzewski, J. Gao, N. Rega, G. Zheng, W. Liang, M. Hada, M. Ehara, K. Toyota, R. Fukuda, J. Hasegawa, M. Ishida, T.

Nakajima, Y. Honda, O. Kitao, H. Nakai, T. Vreven, K. Throssell, J. A. Montgomery, Jr., J. E. Peralta, F. Ogliaro, M. Bearpark, J. J. Heyd, E. Brothers, K. N. Kudin, V. N. Staroverov, T. Keith, R. Kobayashi, J. Normand, K. Raghavachari, A. Rendell, J. C. Burant, S. S. Iyengar, J. Tomasi, M. Cossi, J. M. Millam, M. Klene, C. Adamo, R. Cammi, J. W. Ochterski, R. L. Martin, K. Morokuma, O. Farkas, J. B. Foresman, D. J. Fox, *Gaussian 09, Revision A.02*, Wallingford CT, **2016**.

[42] C. Adamo, V. Barone, *J. Chem. Phys.* **1999**, *110*, 6158–6170.

[43] R. Krishnan, J. S. Binkley, R. Seeger, J. A. Pople, *J. Chem. Phys.* **1980**, *72*, 650–654.

[44] M. J. Frisch, J. A. People, J. S. Binkley, *J. Chem. Phys*. **1984**, *80*, 3265–3269.

[45] T. Cauchy, B. D. Mota, *Quchemreport. A Python Program for Control Quality and Automatic Generation of Quantum Chemistry Results*, **2020**.

[46] N. M. O'Boyle, A. L. Tenderholt, K. M. Langner *J. Comput. Chem.* **2008**, *29*, 839–845.